

Tuning the Electronic and Transport Properties of Penta-Graphene Nanoribbons by Creating Vacancies and Applying an External Electric Field

M. BALVASI* AND A. AVAZPOUR

Physics Department, Faculty of Sciences, Yasouj University, Yasouj, Iran

Received: 21.10.2024 & Accepted: 16.01.2025

Doi: [10.12693/APhysPolA.147.124](https://doi.org/10.12693/APhysPolA.147.124)

*e-mail: mohsen.balvasi@gmail.com

Introducing defect vacancies into nanostructures is a straightforward yet powerful technique employed by scientists to manipulate their properties. In this study, we used a tight-binding model to investigate the effects of an external electric field and the creation of double vacancies at different sites on penta-graphene nanoribbons on the electronic and transport properties. Understanding the effects of external electric fields and vacancy creation on the electronic and transport properties of penta-graphene nanoribbons is important for the advancement of nanoelectronics and the development of innovative applications. After calculating the formation energy for all vacancy structures, it was determined that the maximum stability is achieved when the second vacancy is at the C_2 site. By creating vacancies in the structure, in addition to tuning the energy gap, an indirect-to-direct bandgap transition can be achieved in penta-graphene nanoribbons. The presence of a direct gap in the electronic properties of penta-graphene nanoribbons has significant implications. Direct bandgap materials can absorb and emit photons with energies close to the bandgap energy and may be better suited for optical devices. It was also observed that the creation of vacancies in penta-graphene nanoribbons leads to a phase transition from a semiconductor to a metal. Next, the effect of these vacancies on the transport properties of penta-graphene nanoribbons was investigated. The results clearly show that the maximum current and threshold voltage can be controlled by creating vacancies at various sites on the nanoribbon. In general, by creating double vacancies in the structure or applying an external electric field, an indirect transition to a direct band gap and a semiconductor-to-metal phase transition have been observed. Additionally, when a double vacancy is introduced into the system and an external electric field is applied simultaneously, flat bands are observed in the band structure, as are the tunable band gap, semiconductor-to-metal phase transition, and indirect-to-direct bandgap transition. Additionally, to explore the cause of the change in electronic and transport properties with the creation of a vacancy in the structure, the charge density distribution of carbon atoms was analyzed using density functional theory calculations. Due to the difference in charge density between the penta-graphene nanoribbon sites, significant charge transfer occurs in the structure after a double vacancy is created in the structure. This charge transfer leads to the generation of an electric current in the nanoribbon. Because of these unique characteristics, penta-graphene nanoribbons are promising candidates for the development of solar cells.

topics: penta-graphene nanoribbon, defective vacancies, phase transition, tight-binding approximation

1. Introduction

Over the past decade, there has been significant progress in the development of low-dimensional systems, especially graphene-like materials [1–4], for use in sensors and transistors. Carbon nanostructures are based on pentagons and hexagons. Carbon materials composed of pentagons are rare [5]. A new two-dimensional (2D) carbon allotrope called penta-graphene (PG) was introduced [6]. Penta-graphene has an intrinsic band gap, which makes it a promising material for electronic devices [7]. PG is a carbon allotrope with a 2D pentagonal lattice containing sp_3 -like and sp_2 -like hybridizations

of carbon bonds [7, 8]. The PG is not completely planar, and its 2D projection resembles that of the Cairo tiling, which is composed of fused pentagons [8]. In addition, penta-graphene is a relatively recent topic in materials science, particularly in the study of two-dimensional materials [9, 10].

Penta-graphene nanoribbons (PGNRs) are a new type of two-dimensional material that has attracted much attention in recent years [5, 7]. PGNRs can be obtained by cutting penta-graphene sheets in different crystallographic orientations. The properties of PGNRs can be controlled in a variety of ways, such as by using electric fields, bending, or defects, doping, or changing the edge shapes [7, 11–17]. The mechanical, electronic, optical, and magnetic

properties of PGNRs have been studied by a number of researchers [5, 11, 12, 16, 18–24]. The band gap of PGNRs can be tuned by various methods, and many investigations have been performed to explore the geometry, electronic, and magnetic properties of PGNRs [14]. These studies have shown that PGNRs may have a number of potential applications, including in electronic devices, sensors, and catalysis [9, 24–27]. They have a band gap that is relatively insensitive to the width of the ribbon [25] and, with hydrogenated edges, have a wide range of electronic and magnetic properties [11]. A transverse electric field may promote magnetism in PGNRs and transform magnetic semiconductors into half-metallic wide bandgap materials.

Strain engineering is a key strategy for manipulating magnetic coupling in two-dimensional nanostructures [28–29]. Also, PG can be hydrogenated, fluorinated, or doped with other elements. Quijano-Briones et al. [30] reported that hydrogenating PG sheets doped with Ge and Sn produce stable sheets with a larger band gap than undoped sheets. It is possible to create sheets with desirable properties. The ability to control the properties of PG is a promising development. Ongoing research on PG may uncover additional properties. This could lead to the development of new and exciting applications for PG in the future [30]. Currently, creating defect vacancies in structures is a simple method scientists use to control the properties of nanostructures [31–35]. In this context, extensive theoretical investigations using computational methods such as density functional theory (DFT) have been carried out to explore the effects of external electric fields and vacancy creation on the electronic properties of PGNRs. For example, Manjanathy et al. [31] tuned the electronic and magnetic properties of penta-graphene by creating vacancies in the structure. Additionally, the electronic structures of pristine and vacancy graphene nanoribbons have been investigated using the tight-binding (TB) model [32]. Their results revealed differences between the band structures and the numerical calculation of density of states (DOS) of pristine and defective graphene nanoribbons (GNRs). In addition, the fracture behavior of armchair and defective zigzag graphene nanoribbons was studied [36]. The comparison shows that the effect of vacancies in zigzag graphene nanoribbons is more profound than that in armchair graphene nanoribbons. Generally, the effects of external electric fields and the creation of vacancies on the electronic structure and transport properties of PGNRs have been the subject of significant interest in recent years.

In this study, we employ a TB model to investigate the effects of an external electric field and the creation of vacancies at different possible sites on the electronic structure and transport properties of PGNRs. Understanding how external electric fields and vacancy creation influence electronic structure and transport properties is vital for

designing novel devices based on PGNRs. By manipulating these parameters, researchers can potentially enhance or suppress specific electronic characteristics in PGNRs, including bandgaps, carrier mobility, or even semiconducting-to-metallic transitions. Overall, understanding the effects of external electric fields and vacancy creation on the electronic structure and transport properties of PGNRs is crucial for advancing the field of nanoelectronics and developing innovative applications based on these unique carbon-based materials.

2. Structure and computational method

The atomic configuration of PG is shown in Fig. 1. The methodology is essentially the same as in our previous research [29]. The optimized lattice constants are $a = b = 3.64 \text{ \AA}$, and the side view buckling of $h = 0.6 \text{ \AA}$ shows a 2D sheet with a thickness of 1.20 \AA . The sp_3 and sp_2 hybridizations are denoted as C_1 and C_2 , respectively. The lengths of (C_1-C_2) and (C_2-C_2) bonds are 1.55 \AA and 1.34 \AA , respectively. The origin of the Cartesian coordinate system was chosen to be located at the red atom in the center of the unit cell, and the z -axis is in the direction normal to the PG plane. For simplicity, each atom is labeled with a set (n, m) , where n and m represent the x and y coordinates of the lattice sites, respectively.

2.1. Tight-binding approximation

As mentioned in our earlier work [29], one of the simplest methods for calculating the band structure of a material is the tight-binding approximation (TBA) [37]. The unit cell in Fig. 1 is marked with a square and consists of a C_1 atom and four C_2 atoms. Each C_1 atom in the unit cell is connected to the C_2 atom by the hopping parameter t' . Additionally, each C_2 atom is connected to its nearest neighboring C_2 atom by a hopping parameter t [29]. Also, the on-site energies of carbon atoms C_1 and C_2 are represented as ε_1 and ε_2 , respectively.

In this work, we consider only the nearest neighbors and describe the electronic band structure of PG obtained using the TBA model. The tight-binding Hamiltonian for a PGNR is [38–45]

$$H = \sum_{i,j} t_{i,j} \hat{c}_i^\dagger \hat{c}_j + \sum_i \varepsilon_i \hat{c}_i^\dagger \hat{c}_i + \sum_{i=1}^N U_i \hat{c}_i^\dagger \hat{c}_i, \quad (1)$$

where \hat{c}_i^\dagger (\hat{c}_j) is the creation (annihilation) operator of an electron at site i (j), and $t_{i,j}$ is the hopping energy between sites i and j . The summations run over all site pairs with nonzero hopping. Additionally, ε_i is the on-site energy of the i -th atom, and $U_i = eE_y a_0 y_i$, where e , E_y , and a_0 are the electronic charge, the external transverse electric field,

and the lattice spacing, respectively. By considering the potential difference between the atoms at different sites of the penta-graphene nanoribbon, the role of the external electric field can be simulated. According to the formula $U = -eE_y y$, the transverse electric field leads to the creation of a potential in each unit cell. Therefore, it is enough to adjust the on-site energy value of each atom based on its y coordinate. Finally, the associated potential can be included on the main diagonal of the tight-binding Hamiltonian [5]. Furthermore, when a conductor is subjected to an electric field, the charged particles within it will move in the direction of the field, resulting in the flow of a current in that direction. This principle is explained by Ohm's Law $\mathbf{J} = \sigma \mathbf{E}$ in electromagnetics. Therefore, by applying an external electric field, it is possible to understand the conductivity quality of penta-graphene nanoribbon.

In this work, only nearest neighbor hopping events, including two types of intralayer hopping and one type of interlayer hopping, are considered. We selected the hopping parameters ($t = -3.53$ eV, $t' = 0.26t$) and on-site energies of carbon atoms C_1 and C_2 ($\varepsilon_1 = -0.92$ eV, $\varepsilon_2 = -0.7$ eV) as mentioned in [46]. Using an accurate TB model, the momentum space dispersion of a nanoribbon of PG is calculated directly. We assume that the periodic boundary condition occurs along the ribbon in the x direction. Applying Bloch's theorem and performing the Fourier transformation along the x direction, the Hamiltonian in k space can be written as [38–41]

$$H(k) = H_{00} + H_{01} e^{-ik_x a} + H_{01}^\dagger e^{ik_x a}, \quad (2)$$

where a is the unit-cell length along the x -axis. Additionally, H_{00} and H_{01} describe coupling within a principal unit cell (intra-unit cell) and between adjacent principal unit cells (inter-unit cell), respectively, which can be mapped from the real-space TB model given by (2). Based on the TBA model, the electronic Hamiltonian for the PG in real space can be written as

$$H = \begin{pmatrix} H_{p_1 p_1} & H_{p_1 q_1} & 0 & 0 \\ H_{q_1 p_1} & H_{q_1 q_1} & H_{q_1 p_2} & 0 \\ 0 & H_{p_2 q_1} & H_{p_2 p_2} & H_{p_2 q_2} \\ 0 & 0 & H_{q_2 p_2} & H_{q_2 q_2} \end{pmatrix}, \quad (3)$$

where $H_{p_i p_i(q_i q_i)}$ and $H_{p_i q_i(q_i p_i)}$ are the intra-unit cell and inter-unit cell $(M \times N) \times (M \times N)$ matrices, respectively. In addition, p_i and q_i are sub-cells of the unit cell (see Fig. 1).

2.2. The transport properties of PGNRs using the Landauer formalism

We use Green's function approach for calculating the electronic and transport properties of the PGNRs [47–49]. The Green function of the system is calculated based on the Hamiltonian

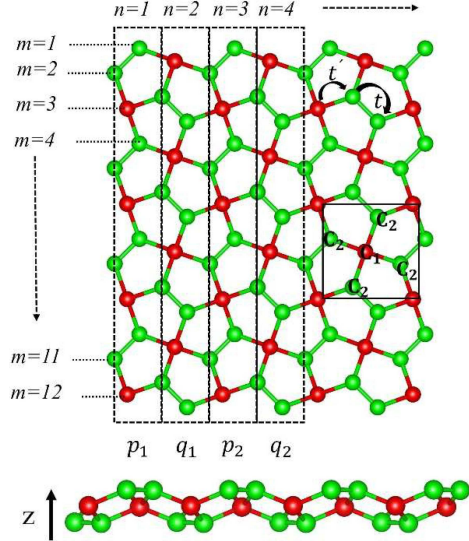


Fig. 1. Top and side views of the PG lattice. The unit cell comprising 6 carbon atoms is enclosed in a black square. Atoms with a coordination number of 4 are labeled C_1 , and those with a coordination number of 3 are labeled C_2 . For simplicity, each atom is labeled with a set (n, m) , where n and m represent the x and y coordinates of the lattice sites, respectively.

through the expression $G = [E - H + i\eta]^{-1}$, where η is a positive infinitesimal number [46]. After Fourier transformation of the Green function in the k -space, the density of states is obtained from $\text{DOS} = -\frac{1}{\pi} \text{Im Tr}[G]$. Next, we investigated transport properties using the TB model and a generalized Green's function method in the Landauer-Büttiker formalism [50–53]. Since transport as a nanoscale phenomenon at low temperature was ballistic [54–56], the current was calculated using the Landauer-Büttiker formula [55–57]

$$I(V) = \frac{2e}{h} \int_{-\infty}^{\infty} dE T(E, V) [f(E - \mu_L) - f(E - \mu_R)]. \quad (4)$$

Here, $f(E - \mu_L)$ and $f(E - \mu_R)$ are the Fermi distribution functions with electrochemical potentials in the left and right leads, respectively, while $T(E, V)$ is the transmission spectrum of incident electrons at energy E and bias V from the left electrode to the right electrode. The electrochemical potential difference between the two electrodes was $\mu_L - \mu_R$. Indeed, the transmission function indicates the rate at which electrons are transmitted from the left to the right electrode by propagation through the molecule. The transmission spectrum and total conductance are obtained from equations [55–57]

$$T(E, V) = \text{Tr} [\Gamma_L(E, V) G(E, V) \Gamma_R G^\dagger(E, V)], \quad (5)$$

$$g = \frac{2e}{h} T(E, V). \quad (6)$$

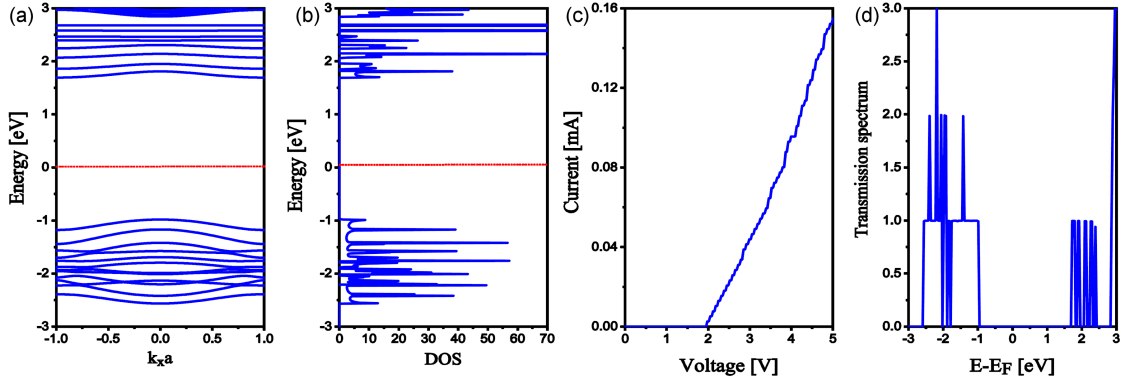


Fig. 2. Electronic and transport properties of PGNRs in the pristine state. The results show that PGNRs are indirect band gap semiconductors with a band gap of 2.67 eV.

In (5)–(6), G^\dagger denotes the advanced and retarded Green functions of the scattering region, while Γ_R and Γ_L are the coupling functions from the right and left electrodes, respectively. In addition, the quantity $g_0 = \frac{2e}{h}$, which is called the conductance quantum, is the natural unit for conductance measurements in mesoscopic systems.

As mentioned in [29], three regions (semi-infinite left electrode, central scattering region, and semi-infinite right electrode) are of the same material (PGNR) (see Fig. 8 in Ref. [29] or see Fig. S1 in Supplementary material). First, we investigated the effect of defect vacancies at different possible sites on the electronic and transport properties of PGNRs. Then, we investigated the effect of an external electric field with different strengths on the electronic and transport properties. Researchers have shown that the C_2 defective penta-graphene structure has a lower formation energy than the C_1 defect structure due to its spontaneous tendency to form sp_3 -like bonds [31]. Therefore, the structural stability of C_2 -mutant penta-graphene is greater than that of C_1 -mutant penta-graphene. However, we considered all the possible sites so that the researchers could find more insight into the creation of vacancies at different sites on the ribbon.

Most of the researchers have focused on studying the properties of a defective penta-graphene structure through the creation of a single vacancy. However, in this study, we have observed no phase transition from semiconductor to metal or from indirect to direct energy gap by creating a single vacancy in the penta-graphene nanoribbon. All these cases are semiconductors with indirect gap and changing energy band gap (see Table SI in Supplementary material). These phase transitions are important in electro-optical and transport applications of nanoribbons. Therefore, our aim in this study is to investigate these phase transitions by creating a double vacancy in the structure, with the goal of providing valuable insights for future researchers in specific applications.

3. Results and discussion

3.1. Effect of vacancy

Usually, atoms that are far from the location where the vacancy is created are not significantly affected by the vacancy. As a result, the system behaves as if it does not have a vacancy. In this study, one of the vacancies is positioned near the center of the nanoribbon cell (site 7). The second vacancy moves across the cell, which consists of 12 atoms. If the location of both vacancies were to be moved across the nanoribbon, a large number of states would need to be checked (a total of 122 states). To reduce complexity, the position of one of the vacancies at site (1, 7) was kept fixed.

In this section, we focus on the effects of creating double vacancies in PGNRs and their impact on the electronic and transport properties. To study the electronic and transport properties of PGNRs, we first calculated the electronic band structure and corresponding density of states for the pristine state. As shown in Fig. 2, PGNR is an indirect band gap semiconductor with a band gap of 2.67 eV. We also find that the peaks and gaps of DOS are in good agreement with the energy bands. In Fig. 2c and d, we present the current–voltage (I – V) curve and transmission spectra $T(E)$ as a function of the electron energy. As shown in Fig. 2, at voltages ranging from 0 to 2 eV, the current is zero, and the material exhibits semiconducting behavior in this system. Hence, the results of the electronic and transport properties in Fig. 2 are consistent.

Subsequently, we explored the effect of the vacancy and the external electric field on the electronic and transport properties of the PGNRs. To clearly understand the effect of vacancies on the band structure, we consider double vacancy defects in the structure in the absence of an external electric field. The first vacancy is fixed at site (1, 7),

TABLE I

Energy gap, formation energy, band gap type, and electronic phase for all the configurations when the first vacancy is fixed at site (1, 7).

Second vacancy site	Carbon atoms	Energy band gap [eV]	Formation energy [eV/atom]	Type of band gap	Electronic phase
(1, 1)	C ₂	2.86	-6.77	indirect	semiconductor
(1, 2)	C ₂		-6.73		metal
(1, 3)	C ₁	1.61	-6.79	direct	semiconductor
(1, 4)	C ₂	2.88	-6.82	indirect	semiconductor
(1, 5)	C ₂		-6.80		metal
(1, 6)	C ₁	1.61	-6.69	direct	semiconductor
(1, 8)	C ₂		-7.00		metal
(1, 9)	C ₁	2.88	-6.70	indirect	semiconductor
(1, 10)	C ₂	2.67	-6.78	indirect	semiconductor
(1, 11)	C ₂		-6.98		metal
(1, 12)	C ₁	1.78	-6.79	direct	semiconductor
pristine structure		2.67	-6.95	indirect	semiconductor

and the second one moves at lattice sites (1, m), where $m = 1, 2, 3, 4, 5, 6, 8, \dots, 12$. These vacancies can be created by removing one C₁ (C₂) atom from the nanoribbon and leaving four (three) nonbonded C atoms. To examine the stability of the PGNRs with double vacancies, we determined the formation energy by using density functional theory (DFT). The calculated values of the double vacancy formation energy are reported in Table I. According to the definition, a more negative value of formation energy indicates a higher level of stability for the structure. Therefore, when the first vacancy is fixed at site (1,7) and the second vacancy is created at sites (1,8) and (1,11), PGNR has excellent stability. Additionally, the maximum stability is achieved when the second vacancy is at the C₂ site. These findings are in good agreement with the results of other studies [31].

The band structure and DOS analysis of Figs. 3 and 4 show that the creation of vacancies in the structure plays an important role in the electronic properties. With the creation of vacancies, the band gap of the defect structures changes. The energy gap values of the structures are listed in Table I. We observe that by creating vacancies in the structure, in addition to tuning the energy gap, an indirect-to-direct bandgap transition can be achieved in PGNRs (see Table I). The presence of a direct gap in the electronic properties of penta-graphene nanoribbons has significant implications and increases their efficiency. Additionally, direct bandgap materials may be better suited for optical devices. As a result, the importance of direct band gap materials for absorbing photons is relatively greater than that of indirect band gap materials. It was also

observed that creating vacancies in the PGNRs results in a phase transition from a semiconductor to a metal (see Table I). This transition represents a significant change in the electronic properties and could have important implications for its potential applications. As shown in Fig. 3, when the first vacancy is fixed at site (1, 7) and the second vacancy is created at sites (1, 2), (1, 5), (1, 8), or (1, 11), a phase transition occurs from a semiconductor to a metal. The transition from a semiconductor to a metal phase is significant because it enables the regulation and manipulation of the electrical conductivity of materials. By managing the transition between the semiconductor and metal phases, engineers can design electronic components with specific features, such as transistors and diodes. Furthermore, this transition is critical in the production of new materials for use in energy-related technologies such as solar cells and batteries. Moreover, the presence of a second vacancy at the (1, 3), (1, 6), and (1, 12) sites leads to an increase in the energy level below the valence bands. Therefore, a tunable band gap is achieved via double vacancy creation. This is important because the tunable bandgap in low-dimensional materials is useful in optoelectronic devices. The DOS curves presented in Fig. 4 provide further evidence for these findings and are in good agreement with the band structure curves shown in Fig. 3.

We explored the effect of these vacancies on the transport properties of the PGNRs. In Figs. 5 and 6, the current-voltage curve and transmission spectra in the presence and absence of an external electric field are plotted. The results of these figures clearly show that the maximum current and threshold

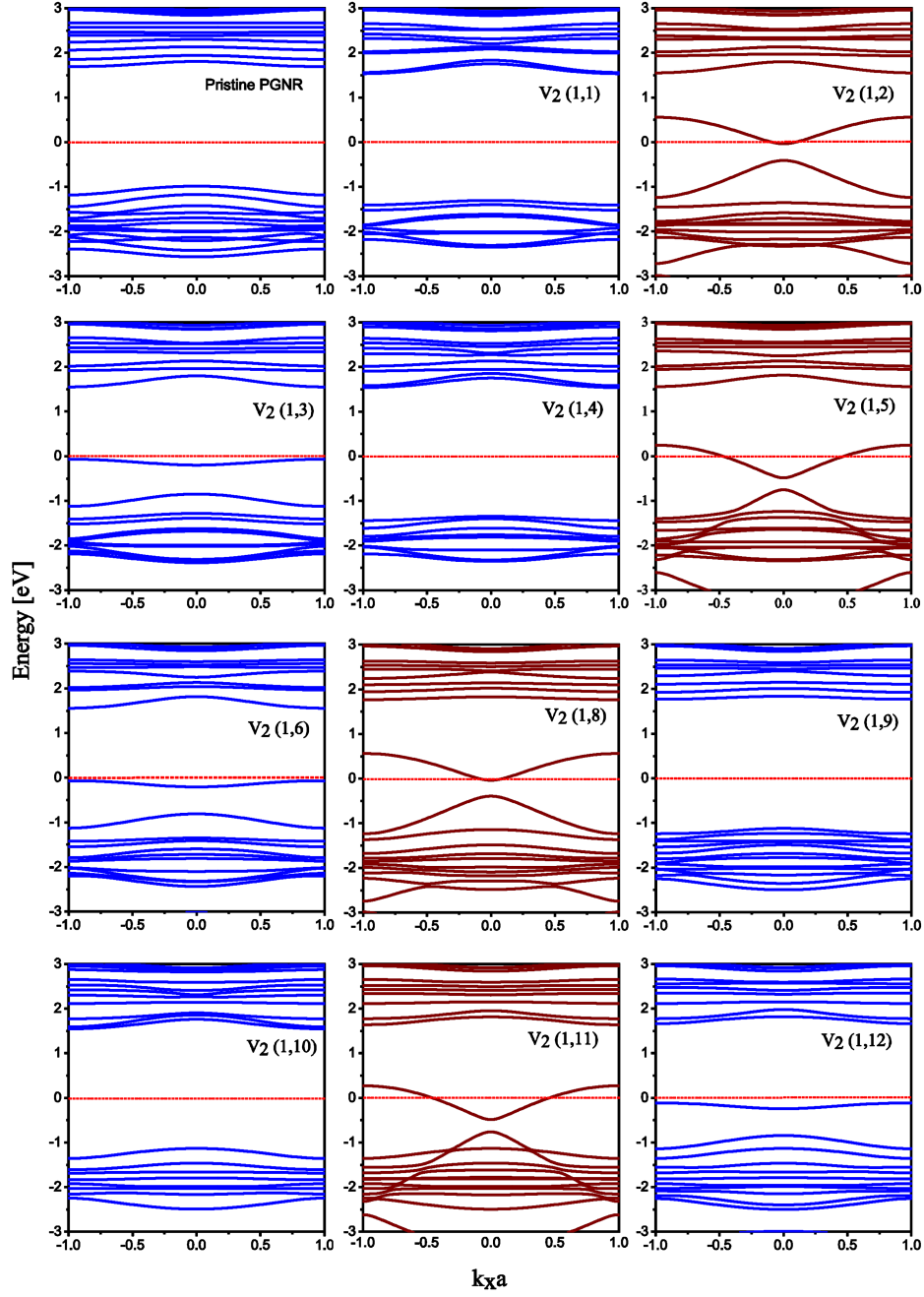


Fig. 3. The band structure for all vacancy structures when the first vacancy is fixed at site (1,7). It can be observed that by creating vacancies in the structure, in addition to tuning the energy gap, an indirect-to-direct bandgap transition and phase transition from a semiconductor to a metal can be achieved in PGNRs.

voltage can be controlled by creating vacancies at various sites on the nanoribbon. Moreover, these diagrams confirm the transition from semiconductor phases to metal phases, which is consistent with the band structure and DOS curves. Generally, the salient results in this section are indirect-to-direct band gap transitions and semiconductor-to-metal phase transitions. It was found that when the semiconducting-to-metal transition occurs, the conduction bands move toward the valence bands, which results in Fermi level crossing. This shift

allows electrons to reach the conduction band more easily and increases the conductivity. In fact, creating vacancies in the system causes changes in the structural symmetry and, as a result, changes in the electron distribution. Hence, creating a second vacancy at sites (1,2), (1,5), (1,8), and (1,11) leads to an increase in electrons in the system, an increase in the electron concentration, and a shift in the Fermi level closer to the conduction band (see Fig. 4). Additionally, the creation of vacancies in these special places is part of *N*-type doping.

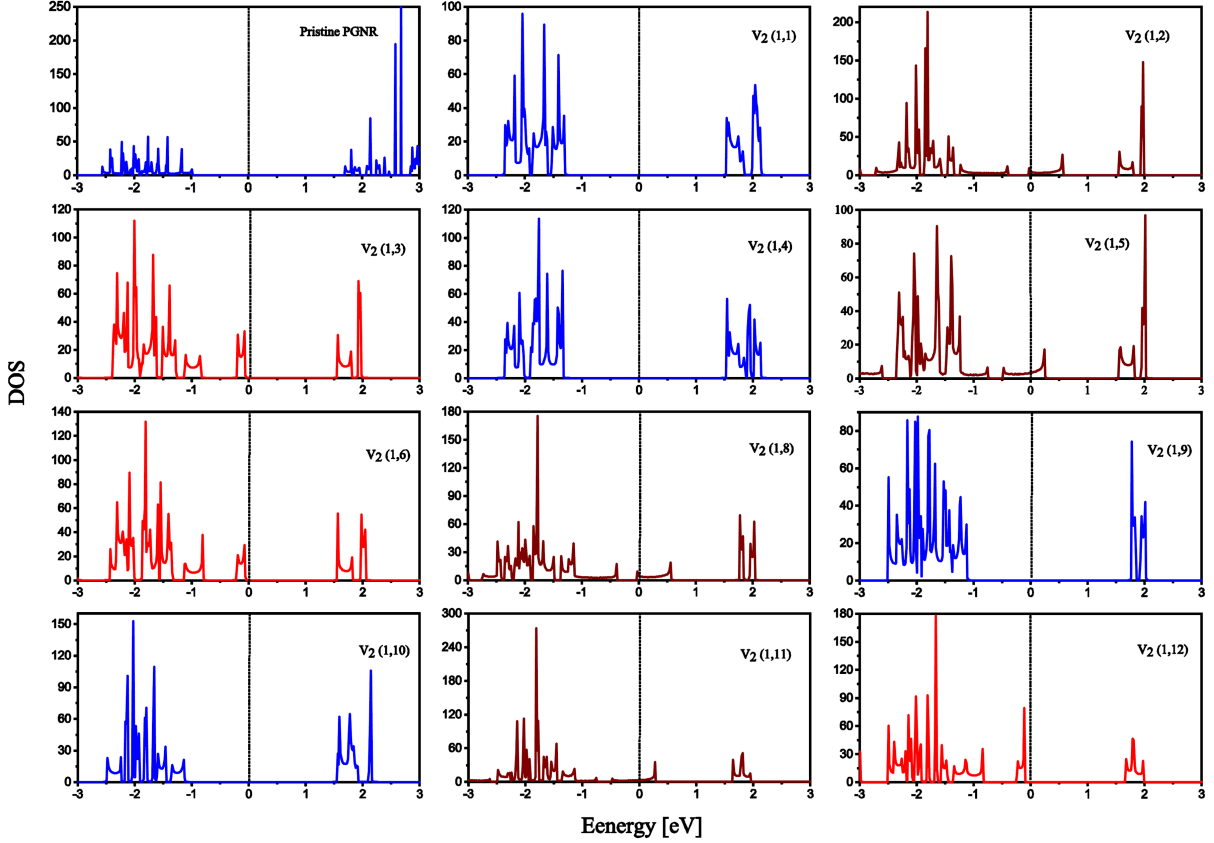


Fig. 4. DOS analysis for all vacancy structures when the first vacancy is fixed at site (1, 7). These findings are in good agreement with the band structure curves shown in Fig. 3.

The creation of a vacancy in penta-graphene leads to a significant change in the charge density distribution of the surrounding carbon atoms. As mentioned earlier, penta-graphene contains both sp_2 and sp_3 bonds. When a vacancy is created at the C_2 (C_1) carbon atom site in this structure, two sp_3 bonds and one sp_2 bond (four sp_3 bonds) are broken, and new hybridizations are formed. For simplicity, the creation of vacancy breaks σ and π bonds, which potentially leads to the induction of states at the Fermi level. This could result in a reduction in the band gap and ultimately lead to a transition from a semiconductor to a metal state. It is important to note that the larger the difference in charge density between two points on the nanoribbon is, the lower the energy required for charge transfer. This charge transfer results in the generation of an electric current within the nanoribbon. This unique characteristic makes penta-graphene nanoribbons a promising candidate for the development of solar cells.

Generally, we have investigated the electronic and transport properties of PG with vacant C sites. The upward movement of valence bands in some areas due to vacancy creation, while remaining unchanged in others, is related to changes in charge density and the type of carbon atom hybridization following the vacancy's formation. The hybridization

state of the carbon atoms adjacent to the vacancies can be altered, affecting the electronic properties of the materials. For example, if a vacancy is created in an sp_2 -hybridized carbon atom, neighboring sp_3 -hybridized carbon atoms may undergo a change in their hybridization state to accommodate the vacancy. This change in hybridization can modify the electronic structure and affect charge transport through changes in bond lengths and angles. In general, the creation of vacancies with different hybridization states in penta-graphene can significantly alter its electron and transport properties by introducing localized states within the bandgap, modifying the hybridization state of neighboring carbon atoms, and increasing scattering events for charge carriers. The creation of a C_2 vacancy leads to each of those three-coordinated atoms in that neighborhood (in the pristine structure) being four-coordinated and becoming C_1 -like.

Additionally, to investigate the cause of the change in electronic and transport properties resulting from the creation of a vacancy in the structure, the charge density distributions of the sp_2 and sp_3 -hybridized carbon atoms were analyzed via DFT calculations (see Figs. S2 and S3 in Supplementary materials). In addition, to better understand the effect of vacancy creation on the electronic and transport properties, the three-dimensional (3D) charge

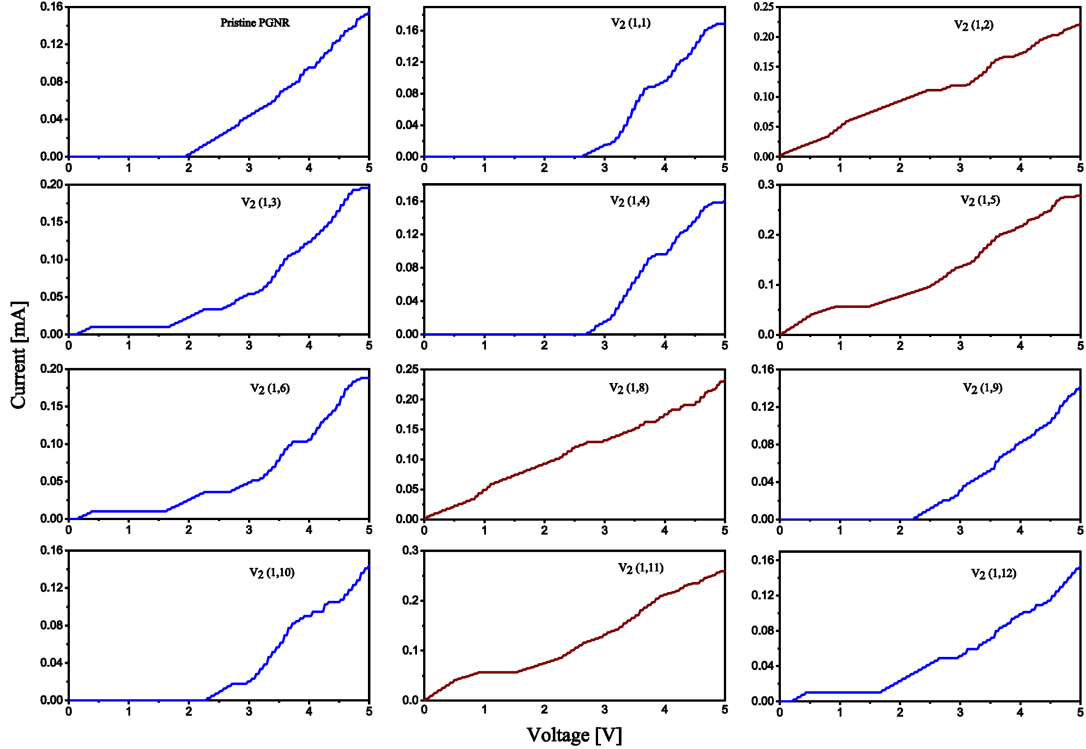


Fig. 5. The I - V curves for all vacancy structures when the first vacancy is fixed at site (1,7). The results show that the maximum current and threshold voltage can be controlled by creating vacancies at various sites on the nanoribbon.

density difference was investigated for two states with and without vacancies (see Fig. 7). In the 3D charge density difference plots (Fig. 7), the yellow and blue regions indicate areas of electron accumulation and depletion, respectively. The analysis of charge density plots indicates that the charge density within sp_3 bonds is lower than that within sp_2 bonds. This difference suggests that the interactions within the sp_2 bonds are stronger than those within the sp_3 bonds. The charge density difference plot of penta-graphene reveals a depletion of charge in the vacancy sites of the lattice, with an accumulation of charge primarily at the bonding sites between the carbon atoms.

Next, for all configurations, the charge transfer (CT) between carbon atoms due to the double vacancy effect was calculated using the Bader charge analysis method. The charge density difference and Bader charge analyses are useful tools for predicting the electron transfer between carbon atoms in PGNRs. The effective charge transfer depends on the vacancy structure, and all the atoms are reconstructed due to dangling bonds around the vacancies (see Fig. S4 in Supplementary materials). These reconstructions change the hybridization and atomic contribution of carbon atoms near the vacancies. Therefore, a two-dimensional charge density distribution is plotted to investigate the variation in charge accumulation due to the vacancy effect. The two-dimensional charge density is plotted

in two figures for each structure around the vacancy regions. In vacancy structures, after force relaxation, all atoms are reconstructed due to dangling bonds around the vacancies. These reconstructions change the hybridization and atomic contribution of carbon atoms near the vacancies. The calculated results illustrated that dangling bonds lead to changes in bond length and charge accumulation. In some structures, carbon atoms attempt to reduce the bond length to attenuate dangling bonds. This effect can be clearly observed from the charge distribution around the carbon atoms of the vacancy. This variation strongly affects the electronic properties of the considered nanoribbons. All the results prove that vacancy creation can be a good strategy for controlling the electronic properties of nanoribbons.

3.2. Effects of external electric field and vacancy

Penta-graphene has a distinct crystal structure characterized by its pentagonal arrangement of carbon atoms. The symmetry of the lattice can lead to certain selection rules for electronic transitions and influence the overall behavior of charge carriers. For example, if certain states are symmetric under specific operations, they may degenerate at high-symmetry points in the Brillouin zone.

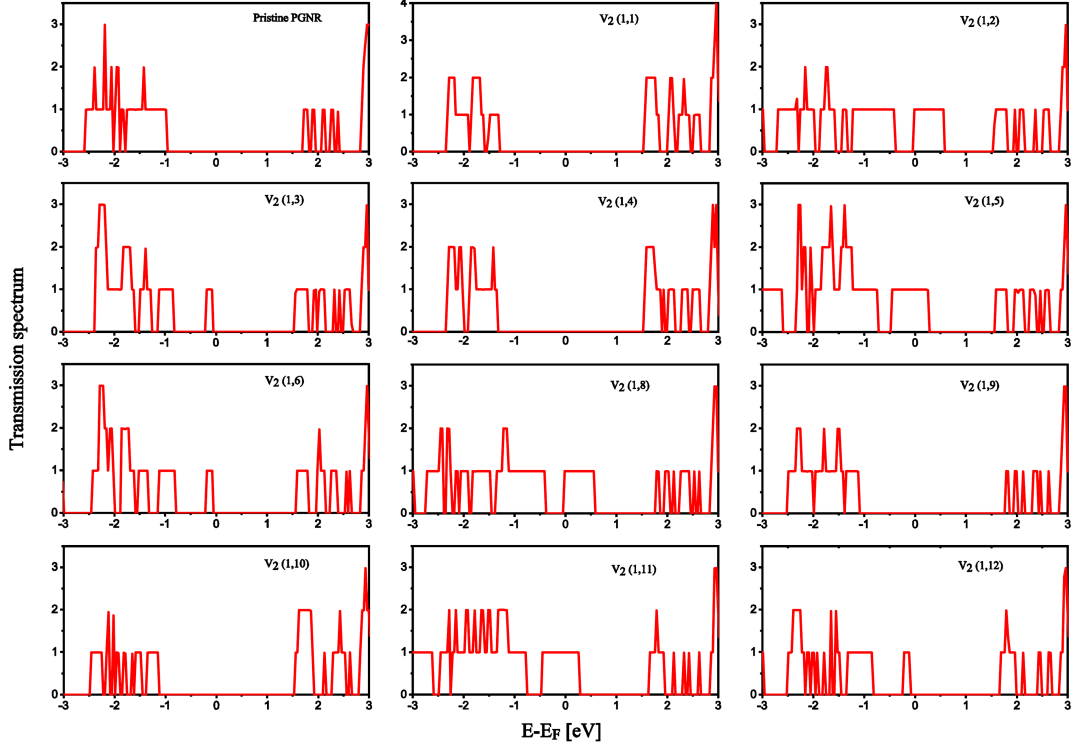


Fig. 6. Transmission spectrum curves for all vacancy structures when the first vacancy is fixed at site (1,7).

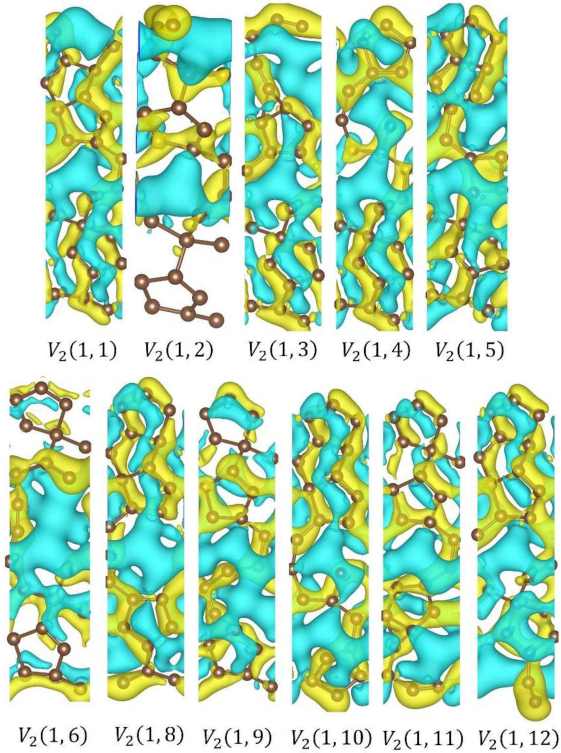


Fig. 7. The three-dimensional (3D) charge density difference of PGNRs was investigated for two states with and without vacancies. When the first vacancy is fixed at site (1,7), the second vacancy moves across the width of the nanoribbon.

Also, the edges of a nanoribbon can break some of the bulk symmetries due to their finite size. For instance, if a penta-graphene nanoribbon is cut along certain crystallographic directions, it may exhibit different edge states that can alter the symmetry properties compared to bulk penta-graphene. In addition, in two-dimensional materials like penta-graphene, energy bands can exhibit degeneracies at specific points in momentum space (the Brillouin zone). For example, at high-symmetry points, bands may be degenerate due to the symmetrical properties of the lattice. Generally, the symmetry properties derived from its unique pentagonal structure play a crucial role in determining its electronic characteristics, and edge effects significantly influence both symmetry and degeneracy. Hence, it is possible that breaking the symmetry and eliminating the degeneracy can be achieved by using the external electric field.

In this section, the effects of applying an external electric field and creating a double vacancy on the electronic and transport properties of PGNRs are examined simultaneously. Applying an external electric field to metal structures cannot be unreasonable because the energy bands may be separated by the application of the electric field, and the transition from the metal to the semiconductor phase may occur. Also, in quantum physics, it is common to eliminate the degeneracy of the energy levels by applying the external electric field to the structure (Stark effect). On the other hand, the conductivity property in a metal can change by changing the

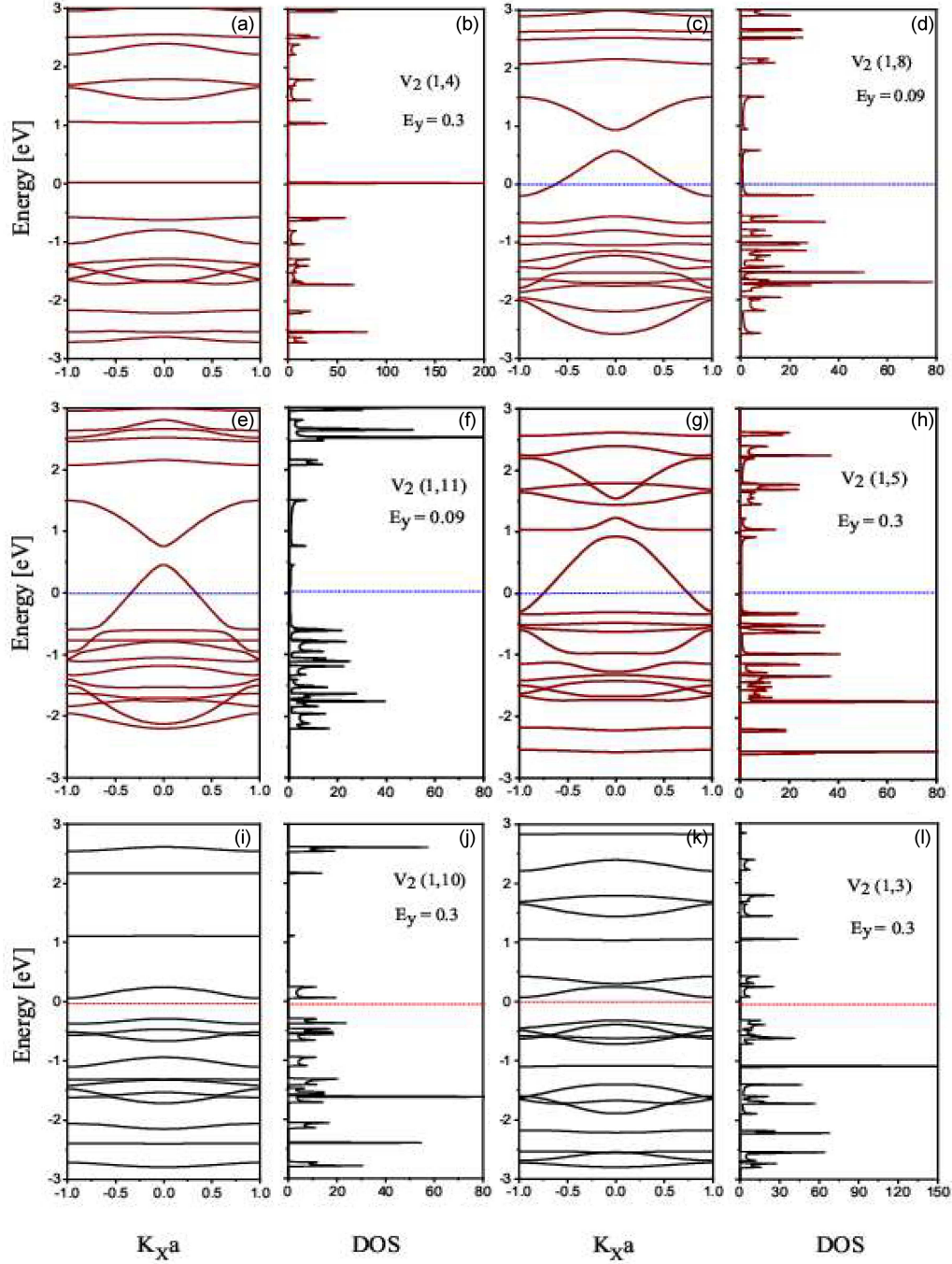


Fig. 8. The band structure and density of states for vacancy structures when the first vacancy is fixed at site (1,7). The computed results show that beyond the tunable band gap, semiconductor-to-metal phase transition, and indirect-to-direct band gap transition, flat bands are generated in the band structures.

slope of the bands because by applying an external electric field, the slope of the energy bands may change, and this leads to an increase or decrease in conductivity in the structure. To explore the electronic properties, the band structure and density of states are shown in Fig. 8. Additionally, Fig. 9 illustrates the I - V characteristics and transmission spectrum of the PGNR. The transverse electric field is applied in the non-periodic direction of the nanoribbon with a unit of $V/\text{\AA}$. Due to the

fact that the coordinates of the atoms are different in the y direction, this field generates a potential difference between the nanoribbon edges. To prevent system disruption due to quantum constraints, external electric field values are kept low (around millivolts per angstrom). By accounting for potential differences across atoms in a penta-graphene nanoribbon, the impact of the external electric field can be modeled. The transverse electric field formula $E_y = -\frac{U}{e_y}$ creates potentials within each unit

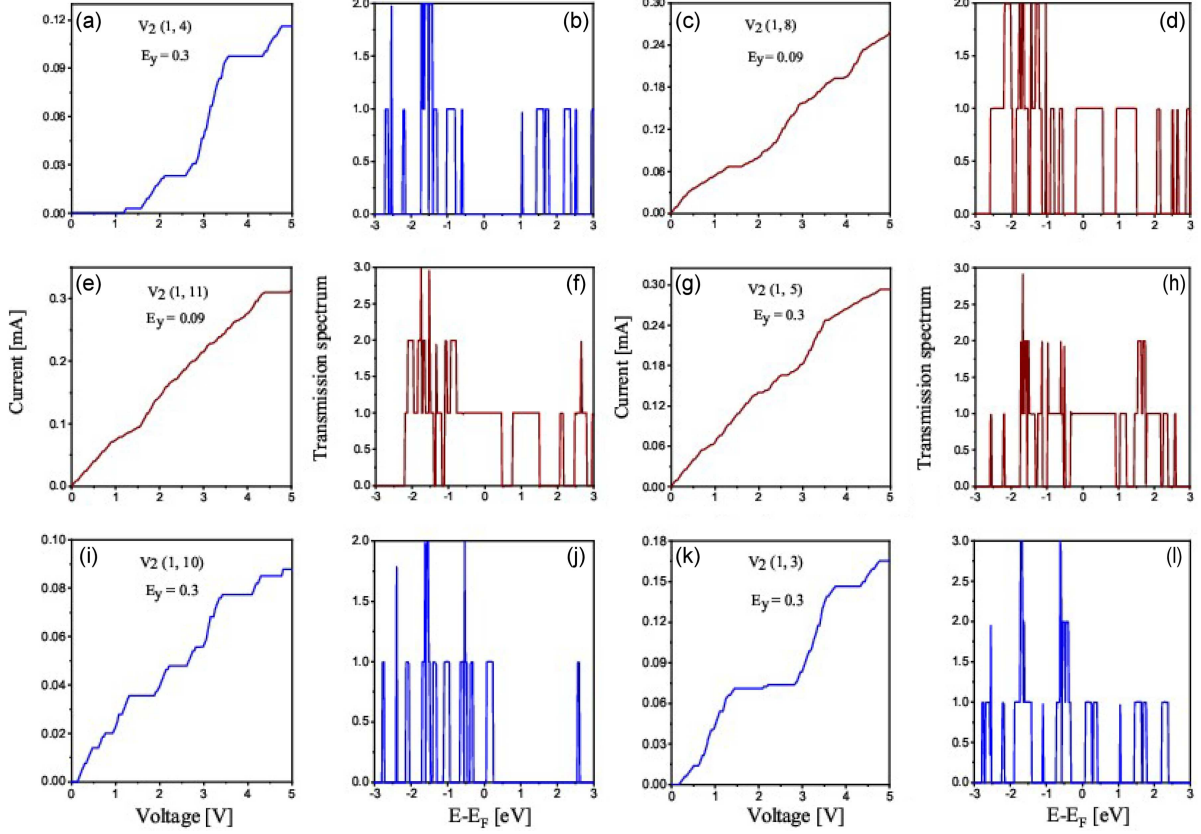


Fig. 9. The I - V curves and transmission spectra for all vacancy structures when the first vacancy is fixed at site (1, 7). The results showed that the maximum current increased from 0.28 mA when there was no external electrical field to 0.29 mA when the effects of the external field and vacancy were considered at the same time.

cell (E_y represents this field). The transverse electric field $\mathbf{E} = (0, E_{\parallel}, 0)$ is actually the component of the field along the y -axis direction. Updating on-site energy based on y coordinates and adding resulting potentials to the tight-binding Hamiltonian's main diagonal is sufficient for simulation [47].

The computed results show that beyond the tunable band gap, semiconductor-to-metal phase transition, and indirect-to-direct band gap transition, flat bands are generated in the band structure (see Fig. 8). A flat band refers to a kind of band structure where the energy remains constant regardless of the crystal momentum. The main characteristic of a flat band is that the particles carrying charge within it possess zero group velocity and an extremely large effective mass. Therefore, a flat band refers to a region in the energy-momentum dispersion relation of a material where the energy is constant regardless of the momentum. The presence of flat bands in band structures is a significant characteristic. When transitioning to flat bands, the electrons become localized. These flat bands have been suggested for use in a field-effect transistor powered by an electric field in the plane. Moreover, flat band systems have attracted interest in different research fields due to their suppressed kinetic energy. The flat bands may arise due to quantum

interference caused by the geometry of the structure. In condensed matter physics, flat bands are considered ideal for studying many-body phenomena such as ferromagnetism, superconductivity, and fractional quantum Hall states [58–59]. For this reason, the carrier kinetic energy in the flat band is subdued and controlled by electron–electron interactions. Flat bands have been studied in several models in three-dimensional, two-dimensional, and one-dimensional structures [60–66]. For example, Moslem Zare [60, 61] showed that nanoribbon structures, such as 2D and Kagome lattices, are inspirational alternatives for creating flat bands. Their results showed the tuning position of the flat band in the presence of mechanical strain and staggered sublattice potential [60, 61]. Additionally, Hien et al. [63] showed that an electronic phase transition and a flat band appear due to strain in phosphorene. Then, we claim that one way to achieve a flat band in PGNRs is to create a double vacancy and apply an external electric field at the same time. Furthermore, one notable achievement is the ability to access the maximum electric current and width of the electron passage channel in the structure by creating a double vacancy and applying an electric field simultaneously. For example, maximum currents of 0.32 mA and 0.29 mA are produced for

$V_2(1, 11)$, $E_y = 0.09$ and $V_2(1, 5)$, $E_y = 0.3$, respectively (see Fig. 9). As illustrated in Fig. 9, the notable occurrence of maximum current values and the distinctive characteristics of the transfer spectrum can be attributed to the migration of valence bands across the Fermi level.

In cases where the semiconducting-to-metal transition has occurred, the valence bands move toward the conduction bands, which results in Fermi level crossing. This shift allows electrons to reach the conduction band more easily and increases the conductivity. Creating vacancies in the system and applying a transverse electric field cause changes in the structural symmetry and, as a result, changes in the electron distribution. Applying a transverse electric field and creating a second vacancy at sites (1, 5), (1, 8), and (1, 11) leads to the creation of holes (absence of electrons) in the valence band and the shift of the Fermi level closer to the valence band (see Fig. 8). Additionally, the application of a transverse electric field and the creation of vacancies in these special places are involved in p-type doping. We believe that our findings provide valuable insight for the application of PGNRs in optoelectronic and electronic devices.

It is worth mentioning that as the transverse electric field increases, the channels in the $T-E$ diagram move closer to the Fermi energy, and their number also increases. Although the height of the channels decreases, greater symmetry is observed. This increase in symmetry allows for more precise control of the current. By applying a transverse electric field, it is possible to achieve transmission of light at the Fermi level and in the vicinity of the Fermi energy. This phenomenon has potential applications in various fields, including optoelectronics and semiconductor technology. In general, the application of an external electric field to the nanoribbon has not significantly improved the realization of the maximum electric current. However, this approach has resulted in the notable effects of shifting the threshold voltage to lower values and shifting transmission spectrum channels to the Fermi level and around it.

4. Conclusions

We used a TB model to investigate the effects of an external electric field and the creation of double vacancies at different sites on the electronic and transport properties of penta-graphene nanoribbons. First, the electronic band structure and corresponding density of states were calculated for the pristine state. According to the results, PGNR is an indirect band gap semiconductor with a band gap of 2.67 eV. After calculating the formation energy for all vacancy structures, it was determined that the maximum stability is achieved when the second vacancy is at the C_2 site. Next, to explore the effect of the vacancy on the electronic and transport

properties of the PGNRs, double vacancy defects at different sites in the structure were considered in the absence of an external electric field. It was observed that by creating vacancies in the structure, in addition to tuning the energy gap, an indirect-to-direct bandgap transition can be achieved in PGNRs. The presence of a direct gap in the electronic properties of penta-graphene nanoribbons has significant implications. Furthermore, the transition from the semiconductor to the metal phases holds immense significance because it enables the design of electronic components with exceptional properties, including transistors and diodes. Moreover, this transition plays a crucial role in the development of novel materials utilized in energy-related technologies, such as solar cells and batteries. Additionally, the obtained results related to the transport properties show that the maximum current and threshold voltage can be controlled by creating vacancies at various sites on the nanoribbon. In fact, the maximum current increases from 0.15 mA in the pristine state to 0.28 mA when a double vacancy is created at sites (1, 7) and (1, 5). Finally, the effects of applying an external electric field and creating a double vacancy on the electronic and transport properties of PGNRs were investigated simultaneously. We find that beyond the tunable band gap, semiconductor-to-metal phase transition, and indirect-to-direct band gap transition, flat bands are generated in the band structures. The presence of flat bands in the band structures of PGNRs is a significant feature. Planar strips are proposed for use in field-effect transistors powered by an in-plane electric field. In addition, flat bands have been suggested for the investigation of many-body phenomena such as ferromagnetism, superconductivity, and the excellent fractional quantum Hall state. The maximum current increases from 0.28 mA in the absence of an external electric field to 0.29 mA in the presence of an external electric field and vacancy at the same time.

To determine the reason for the change in electronic and transport properties resulting from the creation of a vacancy in the structure, the charge density distributions of the sp_2 and sp_3 -hybridized carbon atoms were analyzed via DFT calculations. In addition, the charge transfer (CT) between carbon atoms due to the double vacancy effect was calculated using the Bader charge analysis method. The analysis of charge density plots shows that the charge density within sp_3 bonds is lower than that within sp_2 bonds. This difference suggests that the interactions within the sp_2 bonds are stronger than those within the sp_3 bonds. In vacancy structures, all atoms are reconstructed due to dangling bonds around the vacancies. These reconstructions change the hybridization and atomic contribution of carbon atoms near the vacancies. Due to the difference in charge density between the PGNR sites, significant charge transfer occurs in the structure after a double vacancy is created in the structure. This

charge transfer results in the generation of an electric current within the nanoribbon. Because of these unique characteristics, penta-graphene nanoribbons are good candidates for the development of solar cells.

References

- [1] Ch. Tan, X. Cao, X.J. Wu, Q. He, J. Yang, X. Zhang, J. Chen, W. Zhao, Sh. Han, G.H. Nam, M. Sindoro, H. Zhang, *Chem. Rev.* **117**, 6225 (2017).
- [2] V. Singh, D. Joung, L. Zhai, S. Das, S. Khondaker, S. Sea, *Prog. Mater. Sci.* **56**, 1178 (2011).
- [3] P. Sun, K. Wang, H. Zhu, *Adv. Mater.* **28**, 2287 (2016).
- [4] F. Schwierz, *Nat. Nanotechnol.* **5**, 487 (2010).
- [5] S. Zhang, J. Zhou, Q. Wang, X. Chen, Y. Kawazoe, P. Jena, *Proc. Natl. Acad. Sci.* **112**, 2372 (2015).
- [6] Z. Zhao et al., *J. Am. Chem. Soc.* **134**, 12362 (2012).
- [7] C. He, X.F. Wang, W. X. Zhang, *Phys. Chem. Chem. Phys.* **19**, 18426 (2017).
- [8] N.T. Tien, Ph.T.B. Thao, L.V.Ph. Thuan, D.H. Chuong, *Comput. Mater. Sci.* **203**, 111065 (2022).
- [9] H. Einollahzadeh, S.M. Fazeli, R. Sabet Dariani, *Sci. Technol. Adv. Mater.* **17**, 611 (2016).
- [10] L.A. Openov, A.I. Podlivaev, *Semiconductors* **53**, 717 (2019).
- [11] P.F. Yuan., Z.H. Zhang, Z.Q. Fan, M. Qiu, *Phys. Chem. Chem. Phys.* **19**, 9528 (2017).
- [12] N.T. Tien, P.T.B. Thao, V.T. Phuc, R. Ahuja, *Phys. E Low-Dimen. Syst. Nanostruct.* **114**, 113572 (2019).
- [13] J. Correa, M. Pacheco, S. Bravo, L. Chico, *Carbon* **162**, 209 (2020).
- [14] T. Wu, M. Yao, J. Li, M. Li, M. Long, *Results Phys.* **17**, 103103 (2020).
- [15] N.T. Tien, P. T. B. Thao, V.T. Phuc, R. Ahuja, *J. Phys. Chem. Solids* **146**, 109528 (2020).
- [16] Y. Li, P. Yuan, Z. Fan, Z. Zhang, *Org. Electron.* **59**, 306 (2018).
- [17] V.V. On, L.N. Thanh, N.T. Tien, *Phil. Mag.* **100**, 1834 (2020).
- [18] M. Balvasi, A. Avazpour, J. Jalilian et al., *J. Electron. Mater.* **53**, 834 (2024).
- [19] M. Naseri, S. Lin, J. Jalilian, J. Gu, Z. Chen, *Front. Phys.* **13**, 138102 (2018).
- [20] H. Yuan, Z. Li, J. Yang, *J. Mater. Chem. C* **6**, 9055 (2018).
- [21] L.-S. Zhao, Y. Wang, C.-P. Chen, L.-L. Liu, H.-X. Yu, Y. Zhang, Y. Chen, X.-C. Wang, *Phys. E Low-Dimen. Syst. Nanostruct.* **91**, 82 (2017).
- [22] M.A. Nazir, A. Hassan, Y. Shen, Q. Wang, *Nano Today* **44**, 101501 (2022).
- [23] D.K. Nguyen, N.T.T. Tran, T.T. Nguyen et al., *Sci. Rep.* **8**, 17859 (2018).
- [24] S. Bravo, J. Correa, L. Chico, M. Pacheco, *Sci. Rep.* **8**, 11070 (2018).
- [25] B. Rajbanshi, S. Sarkar, B. Mandal, P. Sarkar, *Carbon* **100**, 118 (2016).
- [26] T.T.T. Hanh, V.K. Dien, N.T.T. Tran, C.H. Ho, T.D.H. Nguyen, M.F. Lin, *Diverse Quasiparticle Properties of Emerging Materials: First-Principles Simulations*, 1st ed., CRC Press, 2022.
- [27] S. Li, Y. Shen, D. Niab, Q. Wang, *J. Mater. Chem A* **9**, 23214 (2021).
- [28] H. Duan, S. Li, S.H. Zheng, Z. Sun, M. Yang, R.Q. Wang, *New J. Phys.* **19**, 103010 (2017).
- [29] M. Balvasi, A. Avazpour, J. Jalilian, M.Z. Bidsardare, *Acta Phys. Pol. A* **144**, 214 (2023).
- [30] J. J. Quijano-Briones, H.N. Fernandez-Escamilla, A. Tlahuice-Flores, *Phys. Chem. Chem. Phys.* **25**, 15505 (2016).
- [31] A. Manjanathy, Ch.P Hsuy, Y. Kawazoe, *2D Mater.* **7**, 045024 (2020).
- [32] K.L. Wong, M.W. Chuan, W.K. Chong, N.E. Alias, A. Hamzah, C.S. Lim, M.L.P. Tan, *Adv. Nano Res.* **7**, 209 (2019).
- [33] M.D Bhatt, H. Kimab, G. Kim, *RSC Adv.* **12**, 21520 (2022).
- [34] K. Tarawneh, A.A. Shukri, Y. Al-Khatatbeh, *J. Electron. Mater.* **52**, 1990 (2023).
- [35] B. Meshginqalam, J. Barvestani, *Appl. Surf. Sci.* **526**, 146692 (2020).
- [36] J. Zhang, T. Ragab, C. Basaran, *Int. J. Damage Mech.* **28**, 325 (2019).
- [37] F. Bloch, *Z. Phys.* **52**, 555 (1929).
- [38] K. Dolui, S. Quek, *Sci. Rep.* **5**, 11699 (2015).
- [39] L.L. Li, D. Moldovan, W. Xu, F.M. Peeters, *Phys. Rev. B* **96**, 155425 (2017).
- [40] M. Zare, *Mater. Res. Express* **6**, 105097 (2019).
- [41] S. Datta, *Quantum Transport-Atom to Transistor*, Cambridge University Press, 2005.

- [42] M. Zare, *J. Appl. Phys.* **128**, 163903 (2020).
- [43] F. Afshari, M. Ghaffarian, *Physica E* **89**, 86 (2017).
- [44] A.N. Rudenko, M.I. Katsnelson, *Phys. Rev B* **89**, 201408(R) (2014).
- [45] S. Shekarforoush1, F. Khoeini, D. Shiri, *Mater. Express* **8**, 489 (2018).
- [46] T.K.Q. Nguyen, T.T. Vu, V.T. Tran, *Semicond. Sci. Technol.* **35**, 095037 (2020).
- [47] M. Zare, E. Sadeghi, *Phys. Rev. B* **98**, 205401 (2018).
- [48] S. Behzad, R. Chegel, *J. Alloys Compd.* **792**, 721 (2017).
- [49] R. Chegel, S. Behzad, *Synth. Met.* **266**, 116476 (2020).
- [50] V.V. On, P.T.B. Thao, L.N. Thanh, N.T. Tien, *AIP Adv.* **12**, 095318 (2022).
- [51] X. Yi, M. Long, A. Liu, S. Zhang, M. Li, H. Xu, *Phys. B Condens. Matter* **595**(15), 412362 (2020).
- [52] M.Q. Cheng, Q. Chen, K. Yang, W.Q. Huang, W.Y. Hu, G.F. Huang, *Nanoscale Res. Lett.* **14**, 306 (2019).
- [53] V. Van On, L.N. Thanh, N.T. Tien, *Phil. Mag.* **14**, 1834 (2020).
- [54] S. Weingart, C. Bock, U. Kunze, F. Speck, Th. Seyller, L. Ley, *Appl. Phys. Lett.* **95**, 262101 (2009).
- [55] M. Büttiker, Y. Imry, R. Landauer, S. Pinhas, *Phys. Rev. B* **31**, 6207 (1985).
- [56] R. Landauer, *IBM J. Res. Dev.* **1**, 223 (1957).
- [57] S. Datta, *Electronic Transport in Mesoscopic Systems*, Cambridge University Press, 1997.
- [58] I. Hase, T. Yanagisawa, Y. Aiura, K. Kawashima, *Phys. Rev. Lett* **120**, 196401 (2018).
- [59] B. Jaworowski, A. Devrim Güçlü, P. Kaczmarkiewicz, M. Kupczyński, P. Potasz, A. Wójs, *New. J. Phys.* **20**, 063023 (2018).
- [60] M. Zare, *Comput. Condens. Matter.* **21**, e00424 (2019).
- [61] M. Zare, *J. Appl. Phys.* **128**, 163903 (2020).
- [62] J.W. Rhim, B.J. Yang, *Adv. Phys. X* **6**, 1901606 (2021).
- [63] N.D. Hien, M. Davoudiniy, K. Mirabbasadeh, L.T.T. Phuong, M. Yarmohammadi, *Chem. Phys.* **522**, 249 (2019).
- [64] R. Khomeriki, S. Flach, *Phys. Rev. Lett.* **116**, 245301 (2016).
- [65] M. Hyrkäs, V. Apaja, M. Manninen, *Phys. Rev. A* **87**, 023614 (2013).
- [66] O. Derzhko, J. Richter, M. Maksymenko, *Int. J. Mod. Phys. B* **29**, 1530007 (2015).